International Journal of Innovative Computing, Information and Control
Volume **15**, Number **6**, December **2019**

 ISSN 1349-4198
pp. **2341–2353**

FINITE-TIME FORMATION CONTROL OF UNMANNED VEHICLES USING NONLINEAR SLIDING MODE CONTROL WITH DISTURBANCES

Honggui Lin[1], Kang Chen[2] and Ruiquan Lin[2,*]

[1]School of Marine Engineering
Jimei University
No. 176, Shigu Road, Xiamen 361021, P. R. China
linhongui36@163.com

[2]College of Electrical Engineering and Automation
Fuzhou University
No. 2, Xueyuan Road, Fuzhou 350116, P. R. China
chenkang123_2003@126.com; *Corresponding author: rqlin@fzu.edu.cn

Received April 2019; revised August 2019

Abstract. *In this paper, a new multi-vehicle formation control method based on second order terminal sliding mode control (SOTSMC) is proposed. The bounded disturbances and uncertainties from modelling and external factors such as gusts and vortices are considered. The conventional sliding mode formation controllers are also investigated and designed. To improve the performance of integral sliding mode controller (ISMC), especially chattering phenomenon and finite-time stability, a second order non-singular terminal sliding mode surface based on an integral sliding surface is introduced to ensure that the nonlinear formation system converges to sliding mode surface from arbitrary initial states in finite time. The Lyapunov stability is proved and total converge time is calculated. Finally, to verify the performance of the proposed SOTSMC formation controller, a comparison between the ISMC and the proposed method is conducted in the simulations with a formation consisting of two followers and one leader which tracks two different prescribed paths.*

Keywords: Multi-agent system, Sliding mode control, Disturbances and uncertainties, Finite-time stability

1. **Introduction.** The multi-agent system (MAS) has drawn a lot of attention since the last decade. As unmanned technology develops rapidly, for instance, unmanned aerial vehicles (UAV), autonomous underwater vehicles (AUV), and mobile robots, formation control problem of MAS has been one of the most important topics for its potential application in military and civil areas, such as swarm combat, cooperative reconnaissance and data collection [1-3]. Due to the nonlinear properties, especially disturbances and uncertainties caused by system modeling, internal vortex and other factors, various control schemes have been adopted in the MAS formation control, which mainly include conventional PID method, robust control, optimal control, adaptive control, sliding mode control (SMC), behavior-based method and so forth [4-10]. In [4], the aerodynamic coupling effects due to the leader's vortices were accurately modeled, and the PI controller was designed in a close leader-follower aircraft formation, but which had poor performance in resisting external disturbances actually. [5] developed a suboptimal controller to deal with external disturbances and model parameter uncertainties in a quadrotor formation

DOI: 10.24507/ijicic.15.06.2341

under a leader-follower framework; however, an exact system model must be known for robust and optimal control, which is hard to be satisfied in practice.

As a common nonlinear control method used in MAS formation control, the sliding mode controller uses the switching between discontinuous control logic to force the control system to move on the sliding mode surface, and to maintain the robustness of the system. It can suppress the uncertainties and disturbances of the system effectively, which also has the advantages of simple structure and quick response [11-16]. In [11], a PID controller was proposed to reject constant disturbances, and an auxiliary integral sliding mode surface was designed to reject the time-varying disturbances in a UAV formation. [12] proposed SMC control laws for multiple unmanned vessels in arbitrary formations with not only mesh and parameter uncertainties but also wave disturbances and mesh unstability. In [13], a fuzzy sliding mode controller was combined with graph theory for a multi-robots system.

However, due to switching motion in the control logic, chattering always happens in sliding mode controllers (including controllers designed in the above studies). Currently, high order sliding mode control (HOSMC) methods can not only eliminate chattering effectively but also maintain the robustness simultaneously, where second order sliding mode controller (SOSMC) applies discontinuous control to the second order derivative of the sliding modulus, which ensures that the sliding modulus and its first order derivative converges to zero and eliminates chattering with advantage. Compared with other high-order sliding mode control, SOSMC is more preferred in practice for its fewer demands on high order information and simple implementation [17-20]. In [17], the first and second order SMC formation controllers were proposed and implemented respectively for cooperative autonomous mobile robots. [19] proposed a robust adaptive satellite formation method by introducing two sliding variables with robust controller and SOSMC.

Finite time convergence is very significant for an MAS formation in most cases [20-24]. However, though SOSMC method based on the linear sliding surface has the ability to eliminate chattering, the time cost of convergence to an equilibrium state cannot be guaranteed to be finite. In [20], an improved terminal sliding mode control (TSMC) method was introduced in multiple under-actuated vehicles system to achieve fast converging without excessive control effort and the singularity problem in conventional TSMC was solved. In [21], an optimal second order sliding mode controller with two different integral sliding mode surfaces was proposed to enhance the robustness of optimal control in a linear uncertain MIMO system.

In this paper, an improved terminal sliding mode formation controller is used for a multi-agent system. The main contribution of this paper is the design of a new finite-time multi-vehicle formation controller using nonsingular second order terminal sliding mode control (SOTSMC) to reject time-varying disturbances and uncertainties and suppress chattering phenomenon with effect in finite time, which can reduce the high-frequency switching loss of executive system devices (such as motors) effectively and shorten the response time. To evaluate the performance of the proposed method, the comparison with a conventional integral SMC formation controller (similar to [10] and [11]) is demonstrated through simulations.

The outline is organized as follows. In Section 2, the problem formulation and system description with disturbances and uncertainties are described. The design of conventional SMC controller and the proposed SOTSMC controller are presented in Section 3. The bounded stability and finite-time convergence are also proved in this section. In Section 4, simulation results and analysis are given to show the effectiveness and advantages of the proposed method. Concluding remarks are provided in Section 5.

2. **Preliminaries and Problem Formulation.** The multi-vehicle formation (e.g. a multiple unmanned vessels formation) under a leader-follower framework is shown in Figure 1. The inertial-fixed frame and body-fixed frame are denoted by x, y and X_B, Y_B respectively and ψ denotes the heading angle with regard to the body frame. Notice that the Follower* denotes the desired state to be achieved for the follower. $\boldsymbol{\xi}$ represents the actual deviations of distance and heading angle in the leader's body-fixed frame between the leader and the ith follower, where $\boldsymbol{\xi}^*$ represents the desired formation geometric parameters. The leader represented by the subscript L is supposed to follow a prescribed trajectory, the followers represented by subscript $i = 1, \ldots, N$ have access to the leader's attitude and position and autonomously maintain a given geometric structure $\boldsymbol{\xi}^*$ with the leader and reach the consensus of velocity vector ultimately. Therefore, the formation problem can be converted to a set of dynamic tracking control problems.

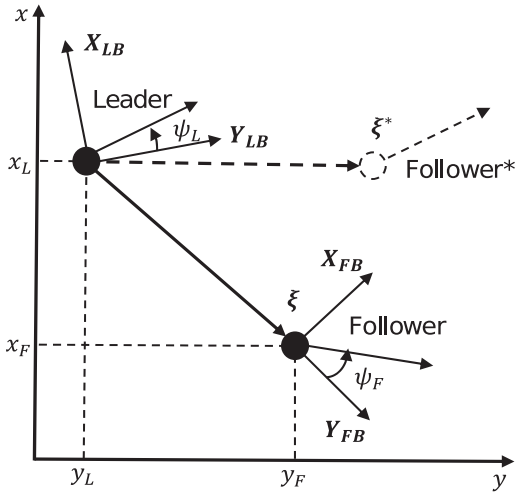

FIGURE 1. Illustration of a leader-follower framework

To study the main aspects of the design of a formation controller, it is assumed that all vehicles are driven by two independent propellers and a bearing regulator, the dynamics model is neglected either. In other words, the formation kinematics model is emphasized in this paper. The kinematic model of the ith vehicle is given as follows [23]:

$$\begin{aligned} \dot{x}_i &= v_{ix} \cos\psi_i - v_{iy} \sin\psi_i \\ \dot{y}_i &= v_{ix} \sin\psi_i + v_{iy} \cos\psi_i \\ \dot{\psi}_i &= \omega_i \end{aligned} \tag{1}$$

where $p_i = [x_i \ y_i]^T$ represents the position of the ith vehicle in the inertial frame, $v_i = [v_{ix} \ v_{iy}]^T$ denotes the linear velocities of the ith vehicle in the body-fixed frame, and ω_i represents the angular velocity of the ith vehicle.

Based on Equation (1), we can get

$$\begin{aligned} v_{ix} &= \dot{x}_i \cos\psi_i + \dot{y}_i \sin\psi_i \\ v_{iy} &= -\dot{x}_i \sin\psi_i + \dot{y}_i \cos\psi_i \end{aligned} \tag{2}$$

Define $\boldsymbol{\xi}_i = [\xi_x \ \xi_y \ \xi_\psi]^T$, considering the disturbances and uncertainties denoted by $\boldsymbol{d} = [d_1 \ d_2 \ d_3]^T$ in the formation flying and modelling, we can get

$$\begin{aligned} \xi_x &= -(x_L - x_i)\cos\psi_L - (y_L - y_i)\sin\psi_L + d_1 \\ \xi_y &= (x_L - x_i)\sin\psi_L - (y_L - y_i)\cos\psi_L + d_2 \\ \xi_\psi &= \psi_L - \psi_i + d_3 \end{aligned} \tag{3}$$

The following formula can be obtained by differentiating Equation (3):

$$\begin{aligned}\dot{\xi}_x &= \xi_y\omega_L + v_{ix}\cos\xi_\psi + v_{iy}\sin\xi_\psi - v_{Lx} + \dot{d}_1\\ \dot{\xi}_y &= -\xi_y\omega_L - v_{ix}\sin\xi_\psi + v_{iy}\cos\xi_\psi - v_{Lx}\dot{d}_2\\ \dot{\xi}_\psi &= \omega_L - \omega_i + \dot{d}_3\end{aligned} \tag{4}$$

Let $\boldsymbol{u} = [v_{ix}\ v_{iy}\ \omega_i]^T$ and $\boldsymbol{D} = \left[\dot{d}_1\ \dot{d}_2\ \dot{d}_3\right]^T$ represent the control input and the derivatives of $\boldsymbol{d}$ of the ith follower respectively, and the formation state functions can be described as follows:

$$\dot{\boldsymbol{\xi}} = \boldsymbol{A} + \boldsymbol{B}u + \boldsymbol{D} \tag{5}$$

where

$$\boldsymbol{A} = \begin{bmatrix} -v_{Lx} + \omega_L\xi_y \\ -v_{Ly} - \omega_L\xi_x \\ \omega_L \end{bmatrix}, \quad \boldsymbol{B} = \begin{bmatrix} \cos\xi_\psi & \sin\xi_\psi & 0 \\ -\sin\xi_\psi & \cos\xi_\psi & 0 \\ 0 & 0 & -1 \end{bmatrix}, \quad \boldsymbol{D} = \begin{bmatrix} \dot{d}_1 \\ \dot{d}_2 \\ \dot{d}_3 \end{bmatrix} \tag{6}$$

Next, we will study the improved sliding mode controller design of nonlinear dynamical system (5) with disturbances and uncertainties.

3. Controller Design and Analysis.

3.1. **Integral sliding mode controller design.** Let $\boldsymbol{\xi}^* = \left[\xi_x^d\ \xi_y^d\ \xi_\psi^d\right]^T$; therefore, the formation tracking error can be described by

$$\boldsymbol{E} = \boldsymbol{\xi}^* - \boldsymbol{\xi} = \begin{bmatrix} \xi_x^d - \xi_x \\ \xi_y^d - \xi_y \\ \xi_\psi^d - \xi_\psi \end{bmatrix} = \begin{bmatrix} e_x \\ e_y \\ e_\psi \end{bmatrix} \tag{7}$$

Consider a proportional integral sliding mode surface given by

$$\boldsymbol{S} = \boldsymbol{E} + \lambda\int_0^t \boldsymbol{E}(\tau)d\tau \tag{8}$$

where $\boldsymbol{S} = [s_x\ s_y\ s_\psi]^T$ is the sliding mode vector and $\lambda = diag[\lambda_1\ \lambda_2\ \lambda_3]$ is a positive real matrix. Assume that the controlled formation would reach sliding mode boundary in finite time under an appropriate control law $\boldsymbol{u}$, let

$$\dot{\boldsymbol{S}} = \dot{\boldsymbol{E}} + \lambda\boldsymbol{E} = 0 \tag{9}$$

Therefore, based on the sliding mode control theory, the according equivalent control law without considering disturbances and uncertainties can be given by

$$\boldsymbol{u}_{eq} = \boldsymbol{B}^{-1}\left(-\boldsymbol{A} + \lambda\boldsymbol{E} + \dot{\boldsymbol{\xi}}^*\right) \tag{10}$$

Remark 3.1. *Apparently, the disturbances and uncertainties in vehicles formation cannot be restrained only by the equivalent control law $\boldsymbol{u}_{eq}$, that is, the nonlinear system (5) cannot be stabilized.*

To decrease the unstability caused by disturbances and uncertainties, a switching control component $\boldsymbol{u}_s$ must be designed to achieve a better formation performance. Hence, Equation (9) can be rewritten as

$$\dot{\boldsymbol{S}} = \dot{\boldsymbol{E}} + \lambda\boldsymbol{E} = \dot{\boldsymbol{\xi}}^* - [\boldsymbol{A} + \boldsymbol{B}(\boldsymbol{u}_{eq} + \boldsymbol{u}_s) + \boldsymbol{D}] + \lambda\boldsymbol{E} = -\boldsymbol{B}\boldsymbol{u}_s - \boldsymbol{D} \tag{11}$$

Using the constant plus proportional reaching law, that is

$$\dot{\boldsymbol{S}} = -\eta\boldsymbol{S} - \rho sgn(\boldsymbol{S}) \tag{12}$$

where η and ρ are positive constant parameters, consequently, we can get the corresponding switching control component as follows:

$$\boldsymbol{u}_s = \boldsymbol{B}^{-1}[\eta \boldsymbol{S} + \rho sgn(\boldsymbol{S})] \tag{13}$$

Theorem 3.1. *The vehicles formation system (8) with disturbances and uncertainties will be achieved asymptotically if the control law is designed as*

$$\boldsymbol{u} = \boldsymbol{u}_{eq} + \boldsymbol{u}_s \tag{14}$$

when $\boldsymbol{D}$ *is bounded and* $\|\boldsymbol{D}\| \leq \rho$.

Proof: Consider a Lyapunov function candidate as

$$V_1 = \frac{1}{2}\boldsymbol{S}^T\boldsymbol{S} \tag{15}$$

Using (11), (13)-(15) yields

$$\begin{aligned} \dot{V}_1 &= \boldsymbol{S}^T\dot{\boldsymbol{S}} \\ &= \boldsymbol{S}^T[-\eta\boldsymbol{S} - \rho sgn(\boldsymbol{S}) + \boldsymbol{D}] \\ &\leq -\eta\boldsymbol{S}^T\boldsymbol{S} - \rho\left|\boldsymbol{S}^T\right| + \left|\boldsymbol{S}^T\right||\boldsymbol{D}| \\ &\leq -\eta\boldsymbol{S}^T\boldsymbol{S}, \text{ when } |\boldsymbol{D}| \leq \rho \end{aligned} \tag{16}$$

Apparently, the nonlinear system (8) under the action of control law (14) satisfies sliding conditions, thus the sliding mode surface becomes an invariant set though disturbances and uncertainties exist. However, the high-frequency chattering is inevitable in the system using control law (14). Next, we will study how to solve this problem.

3.2. **Second order terminal sliding mode control for disturbances.** High order, especially second order terminal sliding mode control (SOTSMC) has been widely used in industrial applications for its high performance in restraining high-frequency chattering, which also needs less high order information. In SOTSMC, the discontinuous control law is used to control the second order derivatives of a given sliding mode surface, which ensures the sliding surface and its first order derivative converge to zero in finite time without chattering. In general, the initial state of a nonlinear system is always outside the sliding surface, according to the terminal sliding mode control theory, arbitrary initial states will converge to the given sliding surface in finite time.

Consider the second order non-singular terminal sliding mode surface based on Equation (8):

$$\boldsymbol{\sigma} = \boldsymbol{S} + \boldsymbol{\gamma}\dot{\boldsymbol{S}}^{\alpha/\beta} \tag{17}$$

where $\boldsymbol{\sigma} = [\sigma_x\ \sigma_y\ \sigma_z\ \sigma_\psi]^T$ and $\boldsymbol{\gamma} = diag[\gamma_1\ \gamma_2\ \gamma_3\ \gamma_4]$ is the chosen switching gain so that $\boldsymbol{\gamma} > 0$, and α and β are selected to satisfy the following conditions:

$$\alpha, \beta \in 2n+1,\ n \in \mathbb{N},\ 1 < \frac{\alpha}{\beta} < 2 \tag{18}$$

Differentiating Equation (17) gives rise to

$$\dot{\boldsymbol{\sigma}} = \dot{\boldsymbol{S}} + \frac{\alpha}{\beta}\gamma\dot{\boldsymbol{S}}^{\alpha/\beta-1}\ddot{\boldsymbol{S}} = \frac{\alpha}{\beta}\gamma\dot{\boldsymbol{S}}^{\alpha/\beta-1}\left(\frac{\beta}{\alpha}\gamma^{-1}\dot{\boldsymbol{S}}^{2-\alpha/\beta} + \ddot{\boldsymbol{S}}\right) \tag{19}$$

Based on Equation (18), we can get

$$\begin{cases} \dot{\boldsymbol{S}}^{\alpha/\beta-1} > 0, \text{ for } \dot{\boldsymbol{S}} \neq 0 \\ \dot{\boldsymbol{S}}^{\alpha/\beta-1} = 0, \text{ for } \dot{\boldsymbol{S}} = 0 \end{cases} \tag{20}$$

Consequently, for Equations (18) and (20), the term $(\alpha/\beta)\,\gamma\dot{\boldsymbol{S}}^{\alpha/\beta-1}$ can be substituted by a positive scalar ζ when $\dot{\boldsymbol{S}} \neq 0$. Therefore, Equation (19) can be rewritten as

$$\dot{\boldsymbol{\sigma}} = \zeta\left(\frac{\beta}{\alpha}\gamma^{-1}\dot{\boldsymbol{S}}^{2-\alpha/\beta} + \ddot{\boldsymbol{S}}\right) \tag{21}$$

Use the constant plus proportional reaching law

$$\dot{\boldsymbol{\sigma}} = -\eta_1\boldsymbol{\sigma} - \rho_1 sgn(\boldsymbol{\sigma}) \tag{22}$$

where η_1 and ρ_1 are positive scalar.

Defining $\eta_2 = \eta_1/\zeta$ and $\rho_2 = \rho_1/\zeta$, based on (21) and (22), we can get

$$\ddot{\boldsymbol{S}} = -\eta_2\boldsymbol{\sigma} - \rho_2 sgn(\boldsymbol{\sigma}) - \frac{\beta}{\alpha}\gamma^{-1}\dot{\boldsymbol{S}}^{2-\alpha/\beta} \tag{23}$$

Differentiating Equation (11) yields

$$\ddot{\boldsymbol{S}} = -\boldsymbol{B}\dot{\boldsymbol{u}}_{s1} - \dot{\boldsymbol{D}} \tag{24}$$

Substituting (23) by (24) yields the control law for disturbances and uncertainties as follows

$$\boldsymbol{u}_{s1} = \int \boldsymbol{B}^{-1}\left(\eta_2\boldsymbol{\sigma} + \rho_2 sgn(\boldsymbol{\sigma}) + \frac{\beta}{\alpha}\gamma^{-1}\dot{\boldsymbol{S}}^{2-\alpha/\beta} - \dot{\boldsymbol{D}}\right) dt \tag{25}$$

where $\left|\dot{\boldsymbol{D}}\right| < \rho_2$.

Remark 3.2. *As for a multi-vehicle formation system, the term $\boldsymbol{D}$ represents the sum of disturbances such as vortex effect caused by neighbor vehicles and uncertainties such as parameters perturbation. However, the formation sampling rate is far larger than the changing rate of $\boldsymbol{D}$ and $\boldsymbol{D}$ is assumed to be invariant in a sampling period, hence $\dot{\boldsymbol{D}} = 0$, that is, the sign function gain ρ_2 can be chosen as $\rho_2 \geq 0$ theoretically, which can eliminate chattering and enhance the control accuracy.*

Note that η_2 determines the convergence rate of the sliding surface. The system states will converge faster with a high value of η_2, which means that it needs higher control inputs and is not much feasible practically. Hence, η_2 must be chosen carefully considering the response speed and control input magnitude.

Thus, the control component (25) can be rewritten as

$$\boldsymbol{u}_{s1} = \int \boldsymbol{B}^{-1}\left(\eta_2\boldsymbol{\sigma} + \rho_2 sgn(\boldsymbol{\sigma}) + \frac{\beta}{\alpha}\gamma^{-1}\dot{\boldsymbol{S}}^{2-\alpha/\beta}\right) dt \tag{26}$$

Theorem 3.2. *The states of vehicles formation system (5) with disturbances and uncertainties can track desired states $\boldsymbol{\xi}^*$ asymptotically if the high order sliding surface is chosen by (17) and the control law is designed as*

$$\boldsymbol{u} = \boldsymbol{u}_{eq} + \boldsymbol{u}_{s1} \tag{27}$$

with $\boldsymbol{D}$ bounded and $|\boldsymbol{D}| \leq \rho$, where $\boldsymbol{u}_{eq}$ is the equivalent control law defined in (10) and $\boldsymbol{u}_{s1}$ is the switching control law defined in Equation (26).

Proof: Consider the Lyapunov function candidate as

$$V_2 = \frac{1}{2}\boldsymbol{\sigma}^T\boldsymbol{\sigma} \tag{28}$$

Differentiating (28) by using (19) yields

$$\dot{V}_2 = \boldsymbol{\sigma}^T\left(\dot{\boldsymbol{S}} + \frac{\alpha}{\beta}\gamma\dot{\boldsymbol{S}}^{\alpha/\beta-1}\ddot{\boldsymbol{S}}\right)$$

$$
\begin{aligned}
&= \boldsymbol{\sigma}^T \left(\dot{\boldsymbol{S}} + \frac{\alpha}{\beta}\gamma \dot{\boldsymbol{S}}^{\alpha/\beta-1} \left(-\boldsymbol{B}\dot{\boldsymbol{u}}_{s1} - \dot{\boldsymbol{D}} \right) \right) \\
&= \boldsymbol{\sigma}^T \left(\dot{\boldsymbol{S}} + \frac{\alpha}{\beta}\gamma \dot{\boldsymbol{S}}^{\alpha/\beta-1} \left(-\left(\eta_2 \boldsymbol{\sigma} + \rho_2 sgn(\boldsymbol{\sigma}) + \frac{\beta}{\alpha}\gamma^{-1}\dot{\boldsymbol{S}}^{2-\alpha/\beta} \right) - \dot{\boldsymbol{D}} \right) \right) \\
&= \frac{\alpha}{\beta}\gamma \dot{\boldsymbol{S}}^{\alpha/\beta-1} \left(-\eta_2 \boldsymbol{\sigma}^T\boldsymbol{\sigma} - \rho_2 \boldsymbol{\sigma}^T sgn(\boldsymbol{\sigma}) - \boldsymbol{\sigma}^T\dot{\boldsymbol{D}} \right) \\
&\le \frac{\alpha}{\beta}\gamma \dot{\boldsymbol{S}}^{\alpha/\beta-1} \left(-\rho_2 |\boldsymbol{\sigma}| - \boldsymbol{\sigma}^T\dot{\boldsymbol{D}} \right) \qquad (29)
\end{aligned}
$$

Choose parameters which satisfy the following condition $0 < \left|\dot{\boldsymbol{D}}\right| < \rho_2$. Moreover, from (25), it is obvious that $(\alpha/\beta)\dot{\boldsymbol{S}}^{\alpha/\beta-1} > 0$, for $\dot{\boldsymbol{S}} \neq 0$. Therefore, the above inequality (29) satisfies

$$\dot{V}_2 < 0, \text{ for } \dot{\boldsymbol{S}} \neq 0 \qquad (30)$$

In other words, the nonlinear system (5) with bounded disturbances and uncertainties is asymptotically stable.

Remark 3.3. *Suppose $\boldsymbol{\sigma}$ reaches zero from $\boldsymbol{\sigma} \neq 0$ in time t_r and $\boldsymbol{\sigma}$ keeps on zero when $t \geq t_r$. Consequently, the control system reaches $\boldsymbol{S} = 0$ in finite time t_s if and only if $\boldsymbol{S}$ reaches $\boldsymbol{S}(t_s) = 0$ from $\boldsymbol{\sigma}(t_r)$, where t_s represents the total time required from $\boldsymbol{\sigma}(0) \neq 0$ to $\boldsymbol{S}(t_s)$. t_s can be calculated as follows.*

Let $\boldsymbol{\sigma} = \boldsymbol{S} + \gamma \dot{\boldsymbol{S}}^{\alpha/\beta} = 0$, hence

$$\dot{\boldsymbol{S}} = -\boldsymbol{S}^{\beta/\alpha}\gamma^{\beta/\alpha} \qquad (31)$$

According to (20), (31) can be rewritten as

$$
\begin{aligned}
\boldsymbol{S}^{\beta/\alpha} &= -\gamma^{\beta/\alpha}\frac{d\boldsymbol{S}}{dt} \\
\text{or } \int_{t_r}^{t_s} dt &= -\gamma^{\beta/\alpha} \int_{\boldsymbol{S}(t_r)}^{\boldsymbol{S}(t_c)} \boldsymbol{S}^{-\beta/\alpha} d\boldsymbol{S} \\
\text{or } t_s - t_r &= -\frac{\alpha}{\alpha-\beta}\gamma^{\beta/\alpha} \left[\boldsymbol{S}(t_r)^{(\alpha-\beta)/\alpha} - \boldsymbol{S}(t_c)^{(\alpha-\beta)/\alpha} \right] \qquad (32)
\end{aligned}
$$

Since $\boldsymbol{S}(t_s) = 0$, (32) gives rise to

$$t_s = t_r + \frac{\alpha}{\alpha-\beta}\gamma^{\beta/\alpha}\boldsymbol{S}(t_c)^{(\alpha-\beta)/\alpha} \qquad (33)$$

Hence, $\boldsymbol{S}$ and $\dot{\boldsymbol{S}}$ converge to zero in finite time.

4. **Simulations.** In this section, the contrastive simulations are conducted between the conventional sliding mode formation controller and second order terminal sliding mode formation controller to verify the performance of the proposed method of this paper.

To validate the performance of second order terminal sliding mode formation controller proposed in this paper, a group of three vehicles in a triangle pattern is considered within a fixed communication network. As shown in Figure 2, the arrows represent that leader's states including position and attitude access to the two followers. The leader initial states are $[x_{L0}\ y_{L0}\ \psi_{L0}\ v_{Lx0}\ v_{Ly0}]^T = [0\ 5\ 0\ 0\ 2]^T$, while the followers initial states are $[x_{F10}\ y_{F10}\ \psi_{F10}\ v_{F1x0}\ v_{F1y0}]^T = [15\ -5\ \pi/2\ 1\ 0]^T$ and $[x_{F20}\ y_{F20}\ \psi_{F20}\ v_{F2x0}\ v_{F2x0}]^T = [-5\ -5\ \pi\ 1\ 1]^T$. The desired formation states for followers are $\xi_1^* = [5\ -5\ 0]^T$ and $\xi_2^* = [-5\ -5\ 0]^T$ respectively. The conventional integral sliding mode controller of $\lambda = 1$, $\eta = 50$ and $\rho = 0.5$ is used as a contrast. The proposed second order terminal SMC

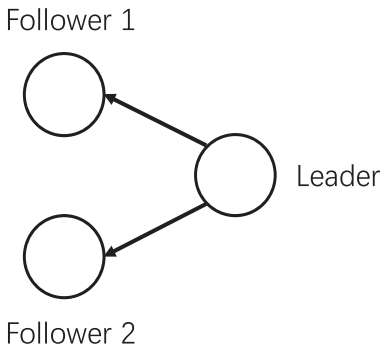

FIGURE 2. Formation communication topology

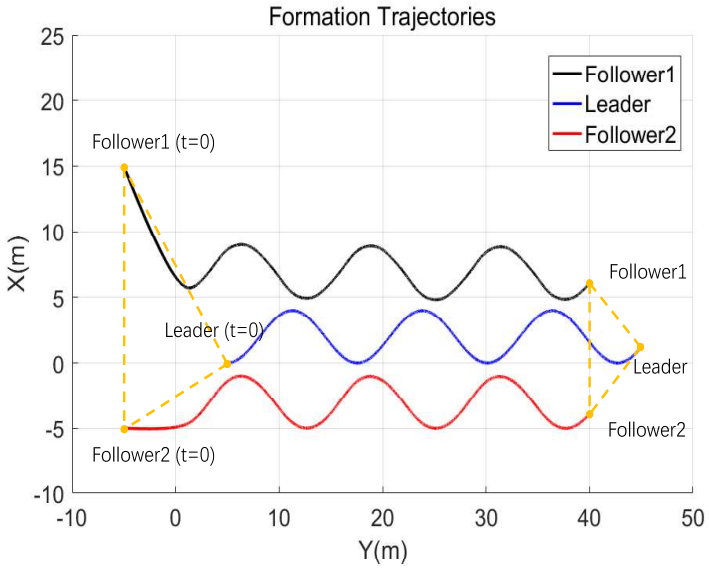

FIGURE 3. (color online) First path: Formation trajectories of three vehicles

controller of $\gamma = diag[8\ 8\ 6]$, $\alpha = 5$, $\beta = 3$, $\eta_1 = 50$, $\rho_1 = 0.5$ and $\zeta = 0.33$ is also applied in the simulations.

4.1. **First path.** The first path to be tracked by the leader can be written as

$$\begin{aligned} x &= 2\cos(t+\pi) \\ y &= 2t+5 \\ \psi &= 0 \end{aligned} \tag{34}$$

Moreover, to simulate the time-varying bounded disturbances and uncertainties $\boldsymbol{D}$ in the formation manoeuvring, the following bounded combinations of trigonometric function are introduced:

$$\begin{aligned} d_1 &= -0.01\cos(0.2t) - 0.03\cos(3t) \\ d_2 &= -0.05\cos t + 0.01\sin(0.1t) \\ d_3 &= 0.05\sin\left(t+\frac{\pi}{3}\right) + 0.01\cos t \end{aligned} \tag{35}$$

Figure 3 shows the trajectories of a three-vehicle formation and all vehicles achieve an equilateral triangle pattern. Figures 4 and 5 indicate the velocities, bearing performance and the tracking error comparison between ISMC and SOTSMC formation controllers.

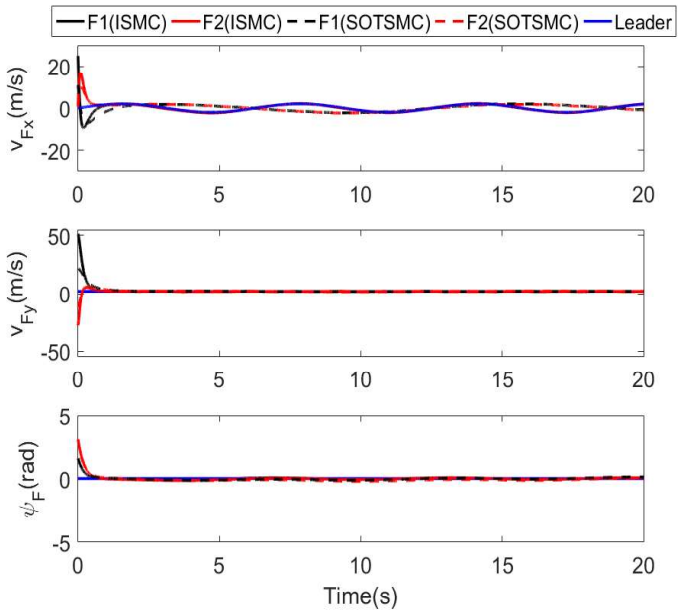

FIGURE 4. (color online) Velocities and bearing performance comparison between ISMC and SOTSMC formation controllers in the first path

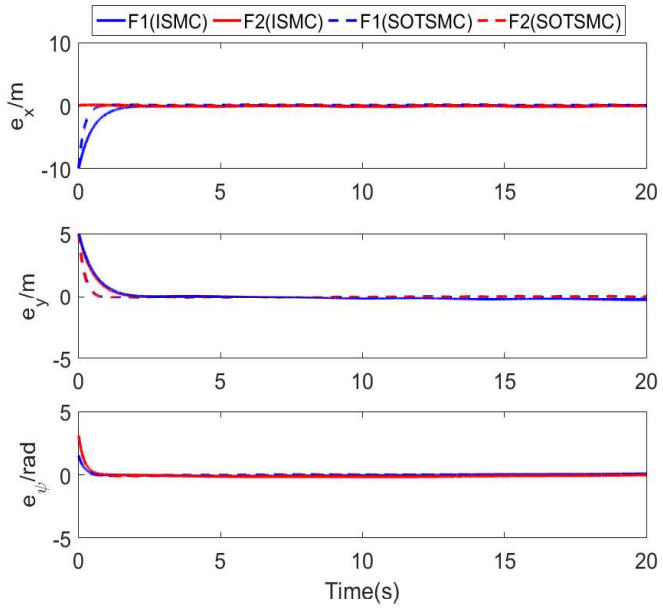

FIGURE 5. (color online) Tracking error comparison between ISMC and SOTSMC formation controllers in the first path

Figure 6 shows the output and sliding mode surface performance comparisons using v_{Fx} as an example, including the local magnification of u_{vFx} when $0.5\text{s} \leq t \leq 1.0\text{s}$.

Obviously, ISMC and SOTSMC controllers can both reject the time-varying bounded disturbances and uncertainties effectively; however, the proposed SOTSMC controller has the advantages of stable output and quick response. For example, the tracking error convergence time of SOTSMC in x and y channel is 1.1s faster than ISMC.

Besides, as shown in Figure 6, the output chattering of u_{vFx} caused by the switching item in Equation (13) still exists in the ISMC controller with an amplitude of 0.8.

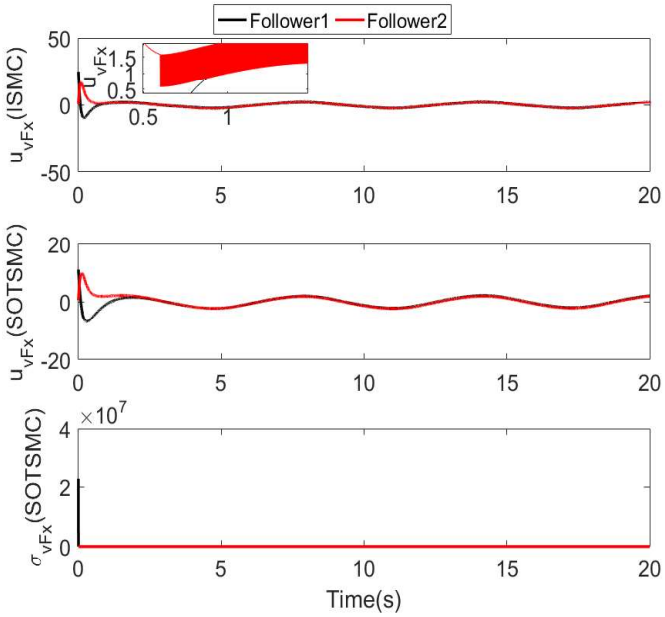

FIGURE 6. (color online) Output performance comparison between ISMC and SOTSMC controller in the first path (using v_{F1x} as an example)

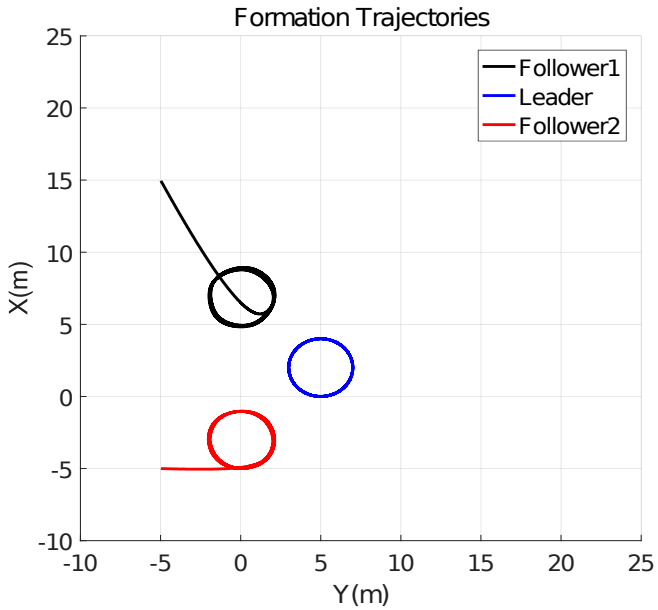

FIGURE 7. (color online) Second path: Formation trajectories of three vehicles

However, the output chattering has already been eliminated in SOTSMC because the discontinuous switching item is working on the second order derivative of the sliding surface. Furthermore, the second order sliding mode surface σ_{vFx} converges to zero instantaneously, which proves the finite time convergence either.

4.2. **Second path.** The second path to be tracked by the leader can be written as

$$\begin{aligned} x &= 2\cos(t+\pi) \\ y &= 2\sin(t)+5 \\ \psi &= 0 \end{aligned} \tag{36}$$

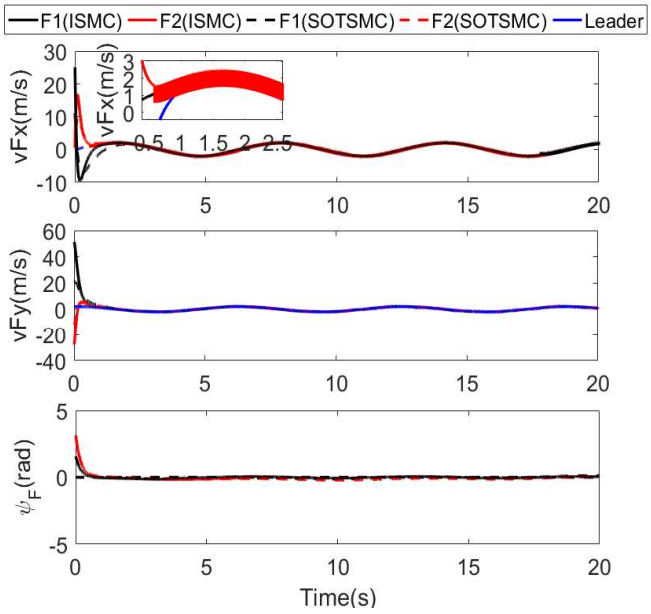

FIGURE 8. (color online) Velocities and bearing performance comparison between ISMC and SOTSMC formation controllers in the second path

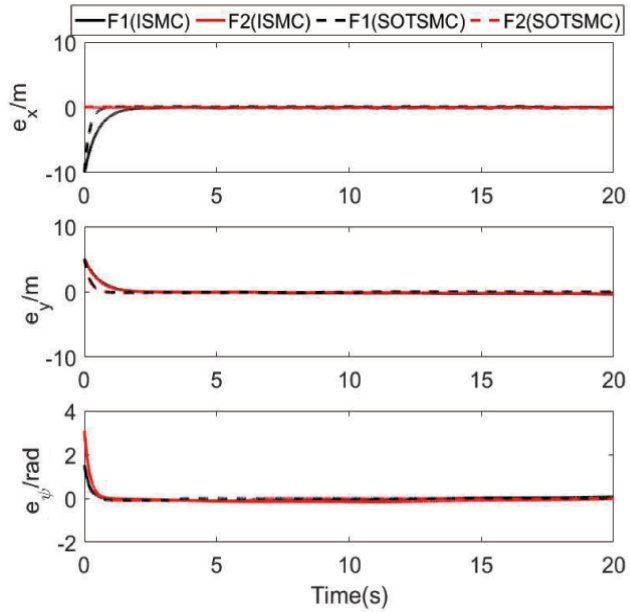

FIGURE 9. (color online) Tracking error comparison between ISMC and SOTSMC formation controllers in the second path

This circular path is much complex than the former path for the whole formation.

The disturbances and uncertainties $\boldsymbol{D}$ in this example are the same as the one introduced in the first case. Figure 7 shows the second formation trajectories; all vehicles move along the circular path and maintain the prescribed triangle formation. Figure 8 and Figure 9 indicate the velocities, bearing performance and the tracking error comparison between ISMC and SOTSMC formation controllers. The local magnification in Figure 8 shows that chattering occurs in the x channel velocity output v_{Fx} of Follower 2 when using ISMC method, while chattering does not happen in the output of SOTSMC.

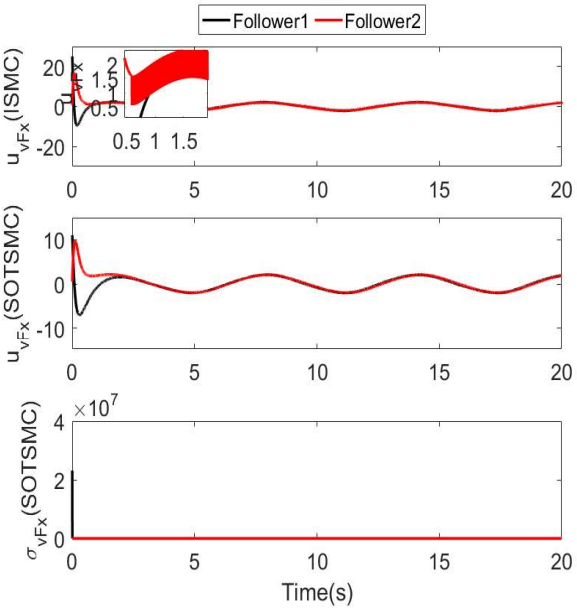

FIGURE 10. (color online) Output performance comparison between ISMC and SOTSMC controller in the second path (using v_{F1x} as an example)

Figure 9 shows the tracking error of SOTSMC controller converges faster than conventional ISMC controller. Figure 10 further implies that the proposed SOTSMC method has advantages in eliminating chattering and finite time convergence.

Based on the results of the above two cases, it is plain to see that the proposed SOTSMC formation controller performs better than conventional SMC controller, which has the value of the practical application.

5. **Conclusion.** This paper mainly contributed a second order terminal sliding mode controller (SOTSMC) for a multi-vehicle formation with bounded disturbances and uncertainties. A second order non-singular terminal sliding mode surface based on the integral sliding mode surface was designed to ensure the nonlinear formation system to converge in finite time, as well as to eliminate the output chattering which always exists in conventional integral sliding mode controller (ISMC). The contrastive simulations verify that the proposed SOTSMC controller outperforms the conventional ISMC in aspects of output stability and convergence time.

Based on the obtained results, several more practical issues such as collision avoidance and communication time delay have not been considered in this work, which will be studied further. Besides, the time-varying communication network will also be taken into account in future work.

Acknowledgment. This work was supported in part by the National Natural Science Foundation of China under Grant No. 61871133, in part by National Natural Science Foundation of Fujian Province under Grant No. 2018J01789 and in part by Minjiang University Open Fund under Grant No. MJXY-KF-EIC1804.

REFERENCES

[1] X. Ge, Q. Han, D. Ding, X. Zhang and B. Ning, A survey on recent advances in distributed sampled-data cooperative control of multi-agent systems, *Neurocomputing*, vol.275, pp.1684-1701, 2018.

[2] M. A. Sayeed and R. Shree, Optimizing unmanned aerial vehicle assisted data collection in cluster based wireless sensor network, *ICIC Express Letters*, vol.13, no.5, pp.367-374, 2019.

[3] B. Zhu, L. Xie, D. Han, X. Meng and R. Teo, A survey on recent progress in control of swarm systems, *Science China Information Sciences*, vol.60, no.7, pp.1-24, 2017.
[4] A. Proud, M. Pachter and J. D'Azzo, Close formation flight control, *AIAA Guidance, Navigation, and Control Conference and Exhibit*, Portland, OR, USA, pp.1231-1246, 1999.
[5] W. Jasim and D. Gu, Robust team formation control for quadrotors, *IEEE Trans. Control Systems Technology*, vol.26, no.4, pp.1516-1523, 2018.
[6] H. Liu, T. Ma, F. Lewis and Y. Wan, Robust formation control for multiple quadrotors with nonlinearities and disturbances, *IEEE Trans. Cybernetics*, pp.1-10, 2018.
[7] J. Wang and M. Xin, Integrated optimal formation control of multiple unmanned aerial vehicles, *IEEE Trans. Control Systems Technology*, vol.21, no.5, pp.1731-1744, 2013.
[8] H. Liang, Z. Sun and J. Wang, Coordinated attitude control of flexible spacecraft formations via behavior-based control approach, *International Journal of Innovative Computing, Information and Control*, vol.8, no.12, pp.8487-8500, 2012.
[9] J. Zhou, Q. Hu and G. Ma, Decentralized adaptive output feedback attitude synchronization tracking control of satellite formation flying, *International Journal of Innovative Computing, Information and Control*, vol.8, no.1(B), pp.977-988, 2012.
[10] M. A. Dehghani and M. B. Menhaj, Integral sliding mode formation control of fixed-wing unmanned aircraft using seeker as a relative measurement system, *Aerospace Science and Technology*, vol.58, pp.318-327, 2016.
[11] R. T. Y. Thien and Y. Kim, Decentralized formation flight via PID and integral sliding mode control, *Aerospace Science and Technology*, vol.81, pp.322-332, 2018.
[12] F. Fahimi, Sliding-mode formation control for underactuated surface vessels, *IEEE Trans. Robotics*, vol.23, no.3, pp.617-622, 2007.
[13] Y. H. Chang, C. W. Chang, C. L. Chen and C. W. Tao, Fuzzy sliding-mode formation control for multirobot systems: Design and implementation, *IEEE Trans. Systems, Man, and Cybernetics, Part B: Cybernetics*, vol.42, no.2, pp.444-457, 2012.
[14] V. Gazi, Swarm aggregations using artificial potentials and sliding-mode control, *IEEE Trans. Robotics*, vol.21, no.6, pp.1208-1214, 2005.
[15] B. Wu, D. Wang and E. K. Poh, Decentralized sliding-mode control for attitude synchronization in spacecraft formation, *International Journal of Robust and Nonlinear Control*, vol.23, no.11, pp.1183-1197, 2013.
[16] J. J. E. Slotine and W. Li, *Applied Nonlinear Control*, Prentice Hall, Englewood Cliffs, NJ, USA, 1991.
[17] M. Defoort, T. Floquet, A. Kokosy and W. Perruquetti, Sliding-mode formation control for cooperative autonomous mobile robots, *IEEE Trans. Industrial Electronics*, vol.55, no.11, pp.3944-3953, 2008.
[18] Z. Wang, F. Guo, Z. Sun, H. Liang and J. Wang, A continuous finite-time attitude synchronization approach for spacecraft formations with communication delays, *International Journal of Innovative Computing, Information and Control*, vol.13, no.3, pp.873-890, 2017.
[19] H. Cho and G. Kersche, Nonlinear robust control for satellite formation flying via adaptive second order sliding modes, *The 27th AAS/AIAA Space Flight Mechanics Meeting*, San Antonio, TX, USA, pp.3641-3654, 2017.
[20] M. Ghasemi, S. G. Nersesov and G. Clayton, Finite-time tracking using sliding mode control, *Journal of the Franklin Institute*, vol.351, no.5, pp.2966-2990, 2014.
[21] M. Das and C. Mahanta, Optimal second order sliding mode control for linear uncertain systems, *ISA Transactions*, vol.53, no.6, pp.1807-1815, 2014.
[22] M. Ghasemi and S. G. Nersesov, Finite-time coordination in multiagent systems using sliding mode control approach, *Automatica*, vol.50, no.4, pp.1209-1216, 2014.
[23] T. Li, R. Zhao, C. L. P. Chen, L. Fang and C. Liu, Finite-time formation control of under-actuated ships using nonlinear sliding mode control, *IEEE Trans. Cybernetics*, vol.48, no.11, pp.3243-3253, 2018.
[24] R. R. Nair, L. Behera and S. Kumar, Event-triggered finite-time integral sliding mode controller for consensus-based formation of multirobot systems with disturbances, *IEEE Trans. Control Systems Technology*, vol.27, no.1, pp.39-47, 2019.